Petroleum Science 20 (2023) 3798–3806

Contents lists available at ScienceDirect

Petroleum Science

journal homepage: www.keaipublishing.com/en/journals/petroleum-science

Original Paper

Catalyst grading technology for promoting the diesel hydrocracking to naphtha

Jia-Qi Ge [a], Peng Zhang [b], Fa-Min Sun [c], Ze-An Xie [d], Zhi-Jie Wu [a], Bai-Jun Liu [a, *]

[a] State Key Laboratory of Heavy Oil Processing, China University of Petroleum, Beijing, 102249, China
[b] Petrochemical Research Institute, PetroChina Company Limited, Beijing, 102206, China
[c] Daqing Petrochemical Research Center, PetroChina Company Limited, Daqing, 163714, Heilongjiang, China
[d] Institute of Catalysis for Energy and Environment, Shenyang Normal University, Shenyang, 110034, Liaoning, China

ARTICLE INFO

Article history:
Received 17 December 2022
Received in revised form
8 February 2023
Accepted 20 May 2023
Available online 20 May 2023

Edited by Jia-Jia Fei

Keywords:
Grading technology
Multi-component catalysts
Hydrocracking
Diesel
Naphtha

ABSTRACT

This paper reports the application of multi-component hydrocracking catalyst grading technology in diesel hydrocracking system to increase naphtha, and studies the influence of catalyst systems with different number of graded beds on the reaction process of diesel hydrocracking. Three hydrocracking catalysts with different physicochemical properties as gradation components, the diesel hydrocracking reaction on catalyst systems of one-component, two-component and three-component graded beds with different loading sequences are carried out and evaluated, respectively. The catalytic mechanism of the multi-component grading system is analyzed. The results show that, with the increase of the number of grading beds, the space velocity of reaction on each catalyst increases, which can effectively control the overreaction process; along the flow direction of feedstock, the loading sequences of catalysts with acidity decreasing and pore properties increasing can satisfy the demand of different catalytic activity for the conversion of reactant with changing composition to naphtha, which has a guiding role in the conversion of feedstock to target products. Therefore, the conversion of diesel, the selectivity and yield of naphtha all increase significantly on the multi-component catalyst system. The research on the grading technology of multi-component catalysts is of great significance to the promotion and application of catalyst systems in various catalytic fields.

1. Introduction

Refining and chemical integration can produce huge synergistic effects and improve the anti-risk ability of enterprises, which has become the development trend of the world petrochemical industry (Popović et al., 2016). Hydrocracking technology has the advantages of wide range of raw materials (Dik et al., 2019; Peng et al., 2018), strong purpose of catalyst system (Angeles et al., 2014), flexible product types and excellent quality (Zhang et al., 2007). It can realize multiple production schemes, such as producing more chemical raw materials (Cao et al., 2022; Sihombing et al., 2020), more jet fuels and more middle distillate oil (Miao et al., 2021). Therefore, the hydrocracking technology can provide strong technical support for the continuous and high-speed development of refining and chemical integration. Catalyst system is the core of hydrocracking technology (Saab et al., 2020), the updating and optimization of which is an effective method to promote the extensive application of hydrocracking technology in refining and chemical integration. Several research institutions (Bellussi et al., 2013; Dai et al., 2016; Dik et al., 2014) have reported that in the fixed bed hydrocracking reactor, the composition of reactants is constantly changing with the direction of feedstock flow, and the single-component catalyst in the traditional hydrocracking technology cannot meet the demand of reactant molecules changing with the reaction for catalyst activity. Therefore, the multi-component catalyst grading technology has gradually been widely concerned by domestic and foreign researchers (Azizi et al., 2013; Peng et al., 2020). The company of Advanced Refining Technologies have successfully developed the Stax technology of catalyst grading (Weng et al., 2020), through two catalysts with high hydrogenation activity and high desulfurization activity, respectively. It is also found that the combining of two catalysts with

* Corresponding author.
E-mail address: bjliu@cup.edu.cn (B.-J. Liu).

https://doi.org/10.1016/j.petsci.2023.05.015

different functions improves the desulfurization efficiency of diesel at different positions in the reactor, and the change of the loading position of the same catalyst will also affect the desulfurization effect of diesel. Threlkel et al. (2010) used the graded combination of desulfurization catalyst and catalytic cracking catalyst to treat the micro-carbon residue and metal components in heavy oil. The results of the test showed that the grading of the two catalysts not only reduced the hydrogen consumption in the reaction process, but also enriched the products in the range of high added value products such as light fraction, gasoline fraction and liquefied petroleum gas. Peng et al. (2016) gradated the Mo–Co catalyst with high trans alkylation performance and W–Mo–Ni catalyst with high hydrogenation activity to improve the desulfurization efficiency. It is found that the raw material passed through the W–Mo–Ni catalyst with high hydro-denitrification activity and the Mo–Co catalyst with high hydrodesulfurization activity successively, which effectively reduced the inhibition of alkylation on nitrides and alleviated the restriction of too high reaction temperature on thermodynamic equilibrium. Therefore, the grading of Mo–Co catalyst and W–Mo–Ni catalyst can more effectively remove the 4, 6-dimethyldibenzothiophene from the feedstock.

To sum up, the current research on catalyst grading technology mainly focuses on catalysts with different functions as grading components, but the research of catalysts with the same function with different activities is rarely involved. Due to the continuous change of the reactant composition in reaction process, the catalyst system including the catalysts with same function, can satisfy the catalytic activity required for the conversion of dynamic reactants to the target product, and provide guidance for the directional conversion of the raw materials. It not only promotes the full conversion of the raw materials, but also facilitate the formation of the target product. Therefore, it is an efficient way to speed up the efficiency of catalytic reaction to conduct gradation research on catalysts with the same function to build a catalyst system highly matched with the reaction process.

In this paper, the grading technology of catalysts with the same function was studied for the first time. Three hydrocracking catalysts with different activities supported by ultra-stable Y zeolite (USY) and amorphous silicon-alumina (ASA) composite materials (Cat-$ASA_{1.7}$, Cat-$ASA_{0.7}$ and Cat-$ASA_{4.0}$) were used as graded components, and with different loading sequences, the single-component catalyst bed, two-component catalyst bed and three-component catalyst bed were designed respectively. The effects of different number of catalyst grading beds and the loading sequence of catalysts on hydrocracking efficiency were discussed. Taking the reaction process of diesel hydrocracking to produce more naphtha as the evaluation system, the effect of different gradation schemes of hydrocracking catalyst on the reaction system was studied through the combined of chromatography and mass spectrometry of products.

2. Experimental

2.1. Catalysts preparation

The catalyst was composed of 22.5 wt% ASA, 30.0 wt% USY, 17.5 wt% alumina sol and 30.0 wt% metal (Ni, W). The USY was mixed with the ASA (molar Si/Al ratio = 0.7, 1.7 and 4.0 respectively), and then mixed with the alumina sol to prepare the composite supports. After that, the composite supports were co-impregnated by the aqueous solution of nickel nitrate and ammonium tungstate with the contents of 6.0 wt% and 24.0 wt% to obtain the catalysts Cat-$ASA_{0.7}$, Cat-$ASA_{1.7}$, Cat-$ASA_{4.0}$.

2.2. Characterization

XRD, Bruker AXSD8 Advance X-ray diffractomet, analyzed the bulk structure of the catalysts; SEM, Quanta 200 (FEI Co., Netherlands), was used to see the surface morphology of catalysts; N_2 adsorption-desorption, Builder KuboX1000, characterized the specific surface area and pore structure of catalysts; Py-IR, VERTEX 80V spectromet, was used fordetecting the total acid and the acid density of catalysts; HRTEM, Philips Tecnai G^2 F20 electron microscopy, was determined the distribution on the catalyst surface.

2.3. Catalytic testing and product analysis

The fixed bed reactor was for testing the catalytic activity of catalyst. In the reactor, the loading modes of single component catalyst, two-component catalyst and three component catalyst were shown in Scheme 1. The bed diameter of all loading modes is 13 mm, and the height of each catalyst bed in the single component catalyst, two-component catalyst and three component catalyst are 40, 20, 13 mm, respectively. In the multi-component catalyst loading modes, the catalyst volume of each bed is same. Quartz wool was added between the catalyst beds to prevent the catalysts from contacting and mixing with each other.

The evaluation process of hydrocracking reaction took diesel as feedstock, naphtha as target product, and the pressure was 6.5 MPa, temperature was 370 °C, the liquid space velocity was 1 h^{-1}, H_2 to diesel ratio was 1000 (*v*/*v*). The properties of feedstock are shown in Table 1. Before reacting, cyclohexane containing 3 wt% CS_2 was used to sulfurize the catalysts. The liquid products were analyzed by chromatography with a simulated distillation packed column. The calculation equations of diesel conversion and naphtha selectivity were as follows. The specific composition of the liquid product was analyzed by the combination of chromatography and mass spectrometry.

$$X_{\text{diesel}}(\%) = \frac{M_{\text{diesel-feed}} - M_{\text{diesel-product}}}{M_{\text{diesel-feed}}} \times 100\% \quad (1)$$

$$S_{\text{naphtha}}(\%) = \frac{M_{\text{naphtha-product}}}{M_{\text{diesel-feed}} - M_{\text{diesel-product}}} \times 100\% \quad (2)$$

where, $M_{\text{diesel-feed}}$, $M_{\text{diesel-product}}$ are the quality of diesel in the feedstock and product, $M_{\text{naphtha-product}}$ is the quality of naphtha in the product.

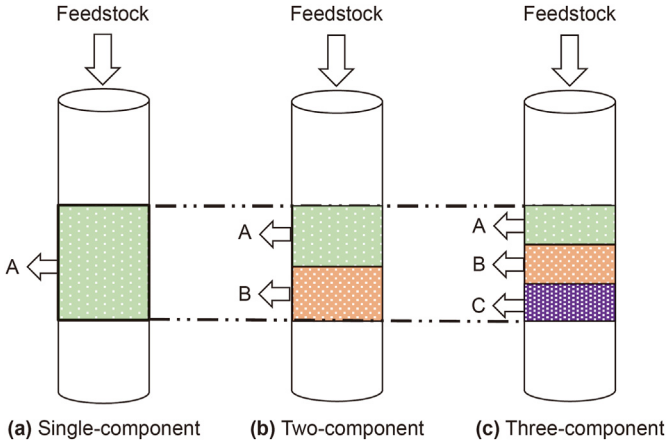

Scheme 1. Loading methods of three different catalyst graded beds.

Table 1
Properties of feedstock.

Characteristic	Value
Boiling range	
IBP/10%	175/221
30%/50%	252/272
70%/90%	294/323
95%/EBP	336/371
Density (20 °C), g/cm^3	0.887
Sulfur content, μg/g	6.1
Nitrogen content, μg/g	4.0

3. Results and discussion

3.1. Characteristics of the catalyst

3.1.1. XRD analysis

Fig. 1 shows the XRD patterns of the catalysts. There are eight typical characteristic peaks of USY on the three catalysts, at 15.7°, 18.7°, 20.4°, 23.6°, 27.1°, 30.8°, 31.5°, 34.2° respectively (Meng et al., 2012). No obvious difference is among the spectra of the catalysts, which indicates there is the similar internal structure of these catalysts (Saab et al., 2020). No characteristic peaks belonging to pure SiO_2, Al_2O_3, metals Ni and W compounds can be observed (Pyagay et al., 2022). It means that the silicon and aluminum species in ASA and aluminum sol in each catalyst exist in amorphous form (Yao et al., 2001), and the crystallite size formed by Ni and W species are too small to be found by XRD device (Zhang et al., 2013).

3.1.2. Texture property

Fig. 2(a) and (b) are the isotherm of adsorption and desorption, the pore size distribution of catalysts respectively. As the Fig. 2(a) shown, all the catalysts have the adsorption isotherm curves of type IV and the hysteresis loops of type H-III, which indicates the existence of mesoporous structures (Tan et al., 2007). Fig. 2(b) is the pore size distribution of catalysts, and the most probable pore size of the catalysts decreases in the order of Cat-$ASA_{0.7}$ > Cat-$ASA_{1.7}$ > Cat-$ASA_{4.0}$. The most probable pore size of Cat-$ASA_{0.7}$ and Cat-$ASA_{1.7}$ catalyst are around 15 and 10 nm respectively, which function well in promoting the diffusion and chemical adsorption of diesel macromolecules (Ding et al., 2016), as well as the accessibility of acid sites (Ivanova et al., 2004; Licea et al., 2014). However, the most probable pore size of Cat-$ASA_{4.0}$ catalyst is only 6 nm, which is due to the enrichment of a large amount of silica colloidal particles with small particle size on the surface of $ASA_{4.0}$ blocking the pore structures (Busca, 2020; Zhu et al., 2018). And the mesoporous structure of catalyst is mainly improved by ASA (Feng et al., 2022; Ge et al., 2022), so the pore size of the Cat-$ASA_{4.0}$ catalyst is smaller than the others.

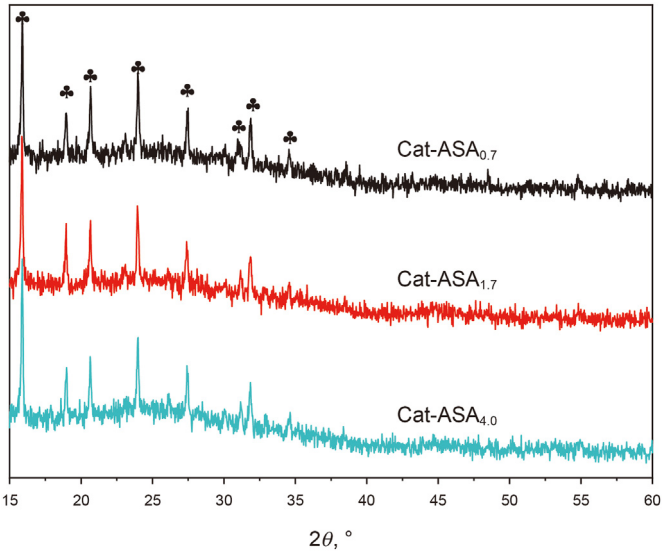

Fig. 1. XRD patterns of the catalysts.

Table 2 is the texture property of the catalysts, which includes the surface area, volume of mesopores (V_{meso}), pore size (d_{mean}) and the V_{meso} content (C_{meso}). The values of these attributes decrease in the order of Cat-$ASA_{0.7}$ > Cat-$ASA_{1.7}$ > Cat-$ASA_{4.0}$, and Cat-$ASA_{0.7}$ catalyst has the best texture properties, especially has the highest surface area, V_{meso} and C_{meso}, which is consistent with the results obtained from Fig. 2(a). The lowest V_{meso} (0.406 g/mL) and C_{meso} (75.0%) means the poor mesoporous characteristics of Cat-$ASA_{4.0}$, which is not conducive to effective internal diffusion and chemical adsorption of diesel macromolecules and is consistent with the pore size distribution in Fig. 2(b).

3.1.3. Acid property

Table 3 is the acid distribution on the catalysts. All the content of Brønsted acid sites (BAS), the B/L value representing the relative content of BAS and the total acid of catalysts decrease in the order of Cat-$ASA_{4.0}$ > Cat-$ASA_{1.7}$ > Cat-$ASA_{0.7}$ at 200 and 350 °C. During testing, as the temperature increases from 200 to 350 °C, the pyridine molecules on the weaker acid sites would be desorbed (Hensen et al., 2010), so the total amount of medium and strong acids measured at 350 °C is positively correlated with the acid strength of the catalyst. The BAS with strong acidity is the main acid sites in the hydrocracking process (Sanchez Escribano et al., 2017), Lewis is the weak acid site (Song et al., 2013), and the Lewis acid sites (LAS) can assist the BAS in raw material processing (Li et al., 2020; Song et al., 2013), so the content of BAS plays an important role on the hydrocracking activity of catalyst. The B/L value is the relative content of BAS and LAS (Zholobenko et al., 2020), the value is related to the synergy between the two acid sites (Guo et al., 2022). Obviously, the acid amount and the acid strength of each catalyst also decrease in the order of Cat-$ASA_{4.0}$ > Cat-$ASA_{1.7}$ > Cat-$ASA_{0.7}$.

Table 4 shows the acid sites density of catalysts, which is obtained by the ratio of the acid amount to the specific surface area of each catalyst. It is the amount of the acid sties on the per unit area of catalysts, and it has been confirmed that it can effectively affect the selectivity of light oil (Derouane et al., 2013; Dik et al., 2019; Liu H. et al., 2022). The density of BAS increases with the increase of the ASA Si/Al ratio (Saber and Gobara, 2014). But the density of LAS is the lowest at the Cat-$ASA_{1.7}$ catalyst, which is consistent with the references (Saber and Gobara, 2014), and it results in the lowest total acid density of this catalyst. Nevertheless, the medium strong acid density of each catalyst tested at 350 °C still decreases in the order of Cat-$ASA_{4.0}$ > Cat-$ASA_{1.7}$ > Cat-$ASA_{0.7}$, which is consistent with the changing trend of BAS density. It means the content of acid sites mainly for cracking process on per unit area of the three catalysts decreases also in the order of Cat-$ASA_{4.0}$ > Cat-$ASA_{1.7}$ > Cat-$ASA_{0.7}$, as does the cracking property (De et al., 2010; Wang et al., 2020).

3.1.4. Surface property

Fig. 3 is the TEM photograph of catalysts in vulcanized state, and the metal sulfide with stacked strip can be seen clearly in every picture. It has been reported that metal components with high hydrogenation activity mostly exist in the corner positions of metal sulfides (Liu et al., 2022; Liu J.X. et al., 2022; Zhou et al., 2018). Therefore, the shorter the strip structure or the more stacking

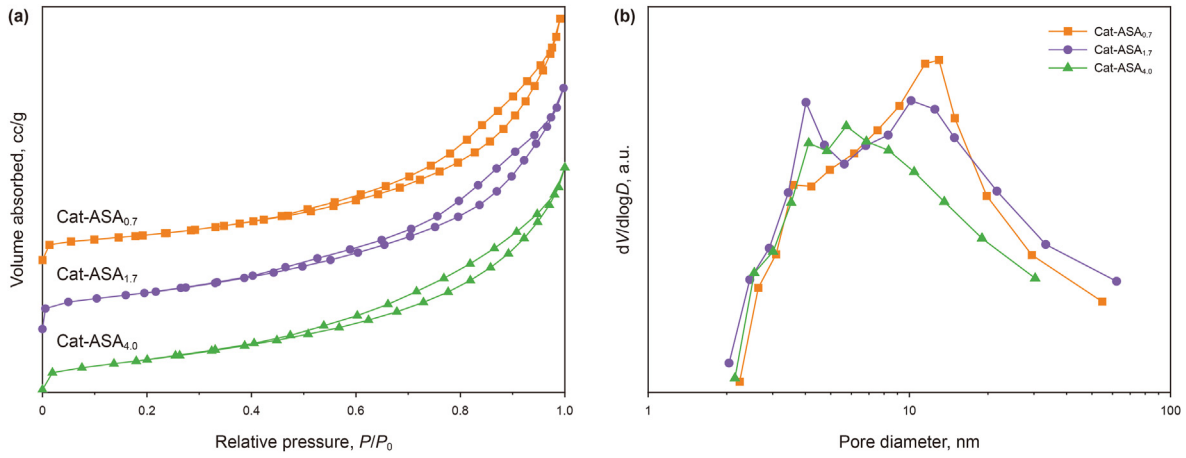

Fig. 2. (**a**) N_2 absorption-desorption isotherms of catalysts; (**b**) Pore size distribution.

Table 2
Preparation of the catalysts under different conditions.

Samples	Surface area, $m^2 \cdot g^{-1}$	Pore volume, $mL \cdot g^{-1}$			d_{mean}, nm	C_{meso}, %
		V_{tatal}	V_{micro}	V_{meso}		
Cat-$ASA_{0.7}$	318	0.746	0.131	0.615	5.48	82.0
Cat-$ASA_{1.7}$	306	0.740	0.148	0.592	5.31	80.0
Cat-$ASA_{4.0}$	263	0.541	0.135	0.406	4.21	75.0

Table 3
Acid distribution of catalysts.

Samples	Amount, μmol/g and distribution of acid sites							
	Total acid (200 °C)				Medium and strong acid (350 °C)			
	B	L	B + L	B/L	B	L	B + L	B/L
Cat-$ASA_{0.7}$	127	546	673	0.233	114	453	567	0.252
Cat-$ASA_{1.7}$	186	491	677	0.379	176	432	608	0.407
Cat-$ASA_{4.0}$	223	539	762	0.414	211	485	696	0.435

Table 4
Acid density distribution of catalysts.

Samples	Acid density, μmol/m^2 and distribution of acid sites							
	Total acid (200 °C)				Medium and strong acid (350 °C)			
	B	L	B + L	B/L	B	L	B + L	B/L
Cat-$ASA_{0.7}$	0.415	1.784	2.199	0.233	0.373	1.480	1.853	0.252
Cat-$ASA_{1.7}$	0.585	1.544	2.129	0.379	0.553	1.358	1.912	0.407
Cat-$ASA_{4.0}$	0.848	2.049	2.897	0.414	0.802	1.844	2.646	0.435

layers of metal sulfides, the more highly active components exist, which means that the stronger the hydrogenation activity of the catalyst (Li et al., 2014; Wang et al., 2020; Yan et al., 2023). The content of metal sulfide with short strip structure and many stacking layers decreases in the order of Cat-$ASA_{0.7}$ > Cat-$ASA_{1.7}$ > Cat-$ASA_{4.0}$, which indicates the hydrogenation activity of the catalyst also decreases in this order (Peng et al., 2022; Voiry et al., 2013).

3.2. Test of grading catalysts bed

3.2.1. Single-component catalyst beds

The hydrocracking activity of the single component catalyst bed is evaluated by the hydrocracking reaction system of diesel. The loading method of the catalyst is shown in Scheme 1(a), and the product distribution is shown in Table 5. The content of gas in the product increases in the order of Cat-$ASA_{0.7}$ < Cat-A $SA_{1.7}$ < Cat-$ASA_{4.0}$, all of which are consistent with acid density and acid strength of the catalyst. Especially the catalyst Cat-$ASA_{4.0}$ with the gas content as high as 18.3%, it has the largest acid density and strongest acid, which provides enough power for cracking (Peng et al., 2022). But the narrow pore structure of catalyst Cat-$ASA_{4.0}$ is not conducive to product diffusion timely, resulting in the continuous cracking of the target product and the generation of gas (Wang et al., 2021). On the contrary, the content of diesel in the product of catalyst Cat-$ASA_{0.7}$ is as high as 20.7%, which means that the conversion of diesel on this catalyst is hindered. Although the good hydrogenation activity of catalyst Cat-$ASA_{0.7}$ can promote in the ring-opening process of fused rings (Song, 2003; Wang et al., 2020), the great structural properties can provide sufficient reaction space for the reaction (Busca, 2019; Perras et al., 2019), but the lowest acid density and worst acid strength cannot provide sufficient active sites and cracking power for diesel conversion.

Fig. 4 shows the hydrocracking activity of a single component catalyst bed. The conversion of diesel on catalyst Cat-$ASA_{0.7}$ is the lowest at 78%, which corresponds to the high diesel content in the product of the catalyst in Table 5. The catalyst Cat-$ASA_{4.0}$ shows the highest diesel conversion rate, but the lowest naphtha selectivity and yield, which confirms again that the target product is over-cracked on this catalyst. The catalyst Cat-$ASA_{1.7}$ has the best catalytic performance, the diesel conversion rate up to 90%, the naphtha selectivity and yield up to 72% and 65%, respectively. It is due to the density of acid sites and acid strength on the catalyst Cat-$ASA_{1.7}$ are only inferior to the catalyst Cat-$ASA_{4.0}$, the texture property and hydrogenation activity are second only to catalyst Cat-$ASA_{0.7}$. Therefore, it has good hydrogenation and cracking activity, as well as sufficient reaction diffusion space, which is not only beneficial to the hydrocracking reaction of diesel, but also helps the products leaving the active site immediately to improve the selectivity of naphtha.

3.2.2. Two-component catalyst beds

The three catalysts Cat-$ASA_{0.7}$, Cat-$ASA_{1.7}$ and Cat-$ASA_{4.0}$ are combined orthogonally in pairs, and the two-component beds of A and B are packed at a volume ratio of 1/1. The packing method is shown in Scheme 1(b). There are three gradation combinations, denoted as Com-1, Com-2 and Com-3, respectively. The acid density and B/L value of these three catalysts decrease in the order of Cat-$ASA_{4.0}$ > Cat-$ASA_{1.7}$ > Cat-$ASA_{0.7}$. Therefore, the loading sequence of

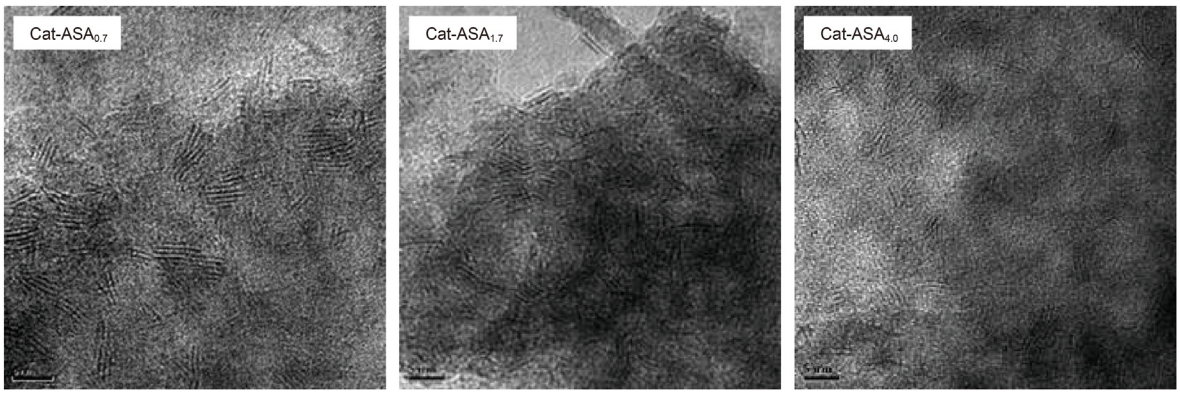

Fig. 3. TEM images of catalysts.

Table 5
Product distribution of diesel hydrocracking on catalysts.

Catalyst	Cat-ASA$_{0.7}$	Cat-ASA$_{1.7}$	Cat-ASA$_{4.0}$
Gas, wt%	6.0	8.6	18.3
Liquid, wt%	94.0	91.4	81.7
Naphtha	73.3	82.2	75.2
Diesel	20.7	9.2	6.5

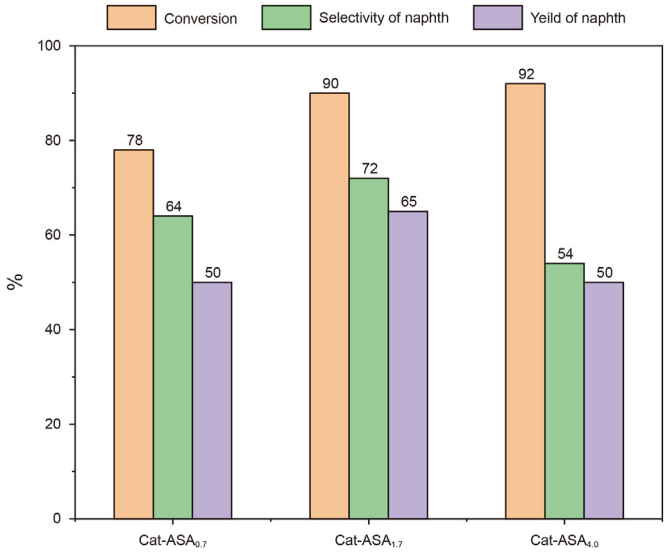

Fig. 4. Diesel hydrocracking activity of catalysts.

increasing catalyst acidity is defined as positive sequence (Com-N) and decreasing catalyst acidity is defined as negative sequence (Com-S) in the logistics direction at all levels. The specific loading method is shown in Scheme 1(b). The gradation combination of each catalyst is shown in Table 6.

Table 7 shows the product distribution results of the diesel hydrocracking reaction in the two-component catalyst gradation system. The gas content in the products of various combinations increases in the order of Com-1 < Com-2 < Com-3, which is consistent with the acidity of the catalysts in the combination, and the naphtha content increases in the order of Com-1 < Com-3 < Com-2. The product distribution of the Com-S grading system is better than that of Com-N, which is shown by the low content of gas and diesel components in the product and the high content of naphtha. This phenomenon occurs in each catalyst combination. According to the characterization results of the catalysts in the preceding part, the reason is that the two catalysts in grading combination form a buffer active channel with strong to weak cracking capacity, and the raw materials through narrow to wide channels, which improves the catalytic efficiency of the grading system.

Fig. 5 shows the evaluation results of diesel hydrocracking reaction activity on the two-component catalyst gradation system. It can be clearly seen that the conversion rate of diesel of all grades combinations decreases in the order of Com-2 > Com-3 > Com-1, and the order of naphtha selectivity and yield is in the order of Com-2 > Com-1 > Com-3 decreasing. The Com-S grading systems have higher catalytic activity than the Com-N, which are consistent with the results in the Table 7. Among them, the Com-2-S combination has the highest catalytic activity, with the diesel conversion rate, naphtha selectivity and yield are as high as 95.0%, 75.0% and 71.0%, respectively.

In the two-component grading system, due to the loading volume of each bed catalyst is only half of the single component bed catalyst, the reaction space velocity is twice that of the single component catalyst bed, which keeps the overreaction process controlled. Furthermore, in the graded bed of Com-S, the acidity of the catalyst decreases with the flow direction of the feedstock, and then the composition of reactants is becoming lighter and lighter. Then, with the increasing pore size, the reactants in feedstock are screened, and the macromolecular substances are preferentially processed (Yue et al., 2017). At the same time, the sufficient pore structure is used to promote product diffusion, which not only promotes the conversion of the diesel and the generation of naphtha, but also alleviates the excessive cracking process. It can be inferred that the catalyst packed in the order of decreasing acidity and increasing texture properties is more conducive to improving the conversion of raw materials and the selectivity of target products.

3.2.3. Three-component catalyst beds

The catalyst Cat-ASA$_{0.7}$, Cat-ASA$_{1.7}$ and Cat-ASA$_{4.0}$ are orthogonally combined as three-component catalysts, and the hydrocracking performance of different gradation methods is studied. The loading of the three-component graded bed is adding the C component of catalyst based on the grading combination of two-component catalyst, and renames it as Com-4, Com-5 and Com-6. Moreover, the loading sequence of catalyst acidity with increasing and decreasing are still marked as Com-N and Com-S, respectively. The specific loading method of the three-component gradation bed of A, B, and C is shown in Scheme 1(c), and the specific catalyst gradation combination is shown in the Table 8.

Table 6
Catalyst combination of two-component graded bed.

Grade bed	Com-1		Com-2		Com-3	
	Com-1-N	Com-1-S	Com-2-N	Com-2-S	Com-3-N	Com-3-S
A	Cat-ASA$_{0.7}$	Cat-ASA$_{1.7}$	Cat-ASA$_{0.7}$	Cat-ASA$_{4.0}$	Cat-ASA$_{1.7}$	Cat-ASA$_{4.0}$
B	Cat-ASA$_{1.7}$	Cat-ASA$_{0.7}$	Cat-ASA$_{4.0}$	Cat-ASA$_{0.7}$	Cat-ASA$_{4.0}$	Cat-ASA$_{1.7}$

Table 7
Product distribution of diesel hydrocracking in two-component graded bed.

Catalyst	Com-1		Com-2		Com-3	
	Com-1-N	Com-1-S	Com-2-N	Com-2-S	Com-3-N	Com-3-S
Gas, wt%	17.6	13.3	20.7	19.3	21.2	23.1
Liquid, wt%	82.4	86.7	79.3	80.7	78.8	76.9
Naphtha	56.9	64.1	72.1	76.7	66.2	72.3
Diesel	25.5	22.5	7.1	4.0	12.6	4.6

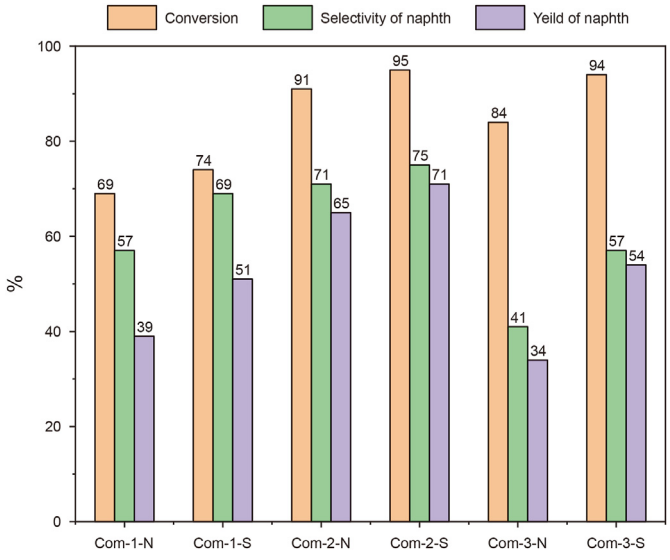

Fig. 5. Diesel hydrocracking activity of two-component graded catalyst beds.

Table 9 shows the distribution results of the diesel hydrocracking reaction products of the three-component catalyst gradation system. It can be found that the gas content in the products increases with Com-6 < Com-5 < Com-4, and the naphtha content decreases with Com-6 > Com-5 > Com-4. Obviously, the catalytic activity order of the three-component gradation combination is Com-6 > Com-5 > Com-4. Compared with the two-component catalyst grading system, the gas content and diesel residue in the product of the three-component catalyst grading system are significantly reduced, while the naphtha content is significantly increased. Only the product of Com-4-N grading combination contains 73.7% naphtha, and the naphtha content of other graded combinations is higher than 80.0%. Among them, the naphtha content of Com-6-S grading combination with the best catalytic performance is as high as 90.3%, while the diesel content is only 2.8%, which is higher than that of the Com-2-S in the two-component grading system.

Table 9
Product distribution of diesel hydrocracking in three-component graded beds.

Catalyst	Com-4		Com-5		Com-6	
	Com-4-N	Com-4-S	Com-5-N	Com-5-S	Com-6-N	Com-6-S
Gas, wt%	18.1	13.8	15.1	9.3	10.0	6.9
Liquid, wt%	81.9	86.2	84.9	90.7	90.0	93.1
Naphtha	73.7	81.0	80.7	83.4	86.4	90.3
Diesel	8.2	5.2	4.2	7.3	3.6	2.8

In addition, the phenomena that the product distribution of Com-S grading system is better than that of Com-N grading system, is more obvious. Similarly, with the two-component grading system, the loading volume of each layer of catalyst further decreases, and the corresponding reaction space velocity increases, which shorts the contact time between each layer of catalyst and feedstock, so effectively prevents the occurrence of overreaction process. In addition, in the flowing direction of feedstock, the grading channel, with catalyst acidity decreasing and pore structure increasing, is denser and then promotes the conversion of diesel to naphtha.

Fig. 6 shows the diesel hydrocracking activity of the three-component catalyst gradation system. It can be seen from the figure that the diesel conversion rate on each combination is higher than 90.0%, but the selectivity and yield of naphtha decrease in the order of Com-6 > Com-5 > Com-4. The reverse sequence scheme Com-S in each combination has higher diesel conversion rate, naphtha selectivity and yield than that of the positive sequence loading scheme Com-N, which is consistent with the two-component graded bed. The gradation combination Com-6-S with decreasing acidity and increasing texture properties of the catalyst shows the best diesel hydrocracking activity, its diesel conversion rate is as high as 97.0%, and the selectivity and yield of naphtha up to 78.0% and 76.0%, respectively, which is much higher than that of the Com-2-S.

3.3. Mechanism analysis

In order to explore the hydrocracking activity mechanism of the multi-component catalyst grading system, we conducted a test of bed decline layer-by-layer on the grading combination Com-6-S with the best catalytic activity, and completed the catalytic

Table 8
Catalyst combination of three-component graded bed.

Grade bed	Com-4		Com-5		Com-6	
	Com-4-N	Com-4-S	Com-5-N	Com-5-S	Com-6-N	Com-6-S
A	Cat-ASA$_{0.7}$	Cat-ASA$_{1.7}$	Cat-ASA$_{0.7}$	Cat-ASA$_{4.0}$	Cat-ASA$_{1.7}$	Cat-ASA$_{4.0}$
B	Cat-ASA$_{1.7}$	Cat-ASA$_{0.7}$	Cat-ASA$_{4.0}$	Cat-ASA$_{0.7}$	Cat-ASA$_{4.0}$	Cat-ASA$_{1.7}$
C	Cat-ASA$_{4.0}$	Cat-ASA$_{4.0}$	Cat-ASA$_{1.7}$	Cat-ASA$_{1.7}$	Cat-ASA$_{0.7}$	Cat-ASA$_{0.7}$

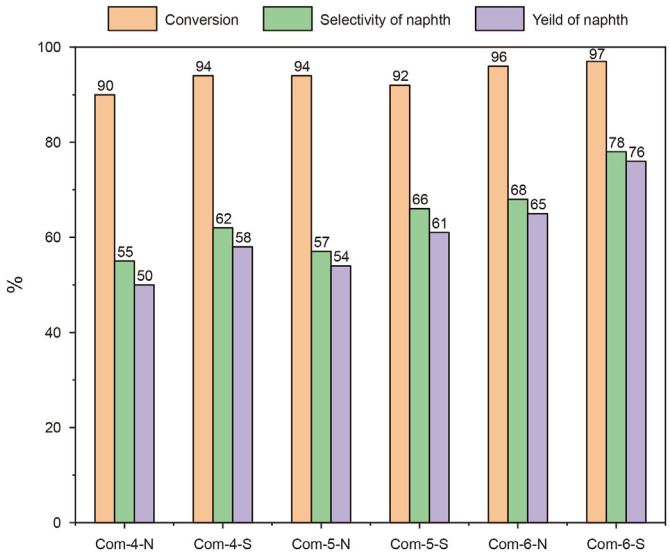

Fig. 6. Diesel hydrocracking activity of three-component graded catalyst beds.

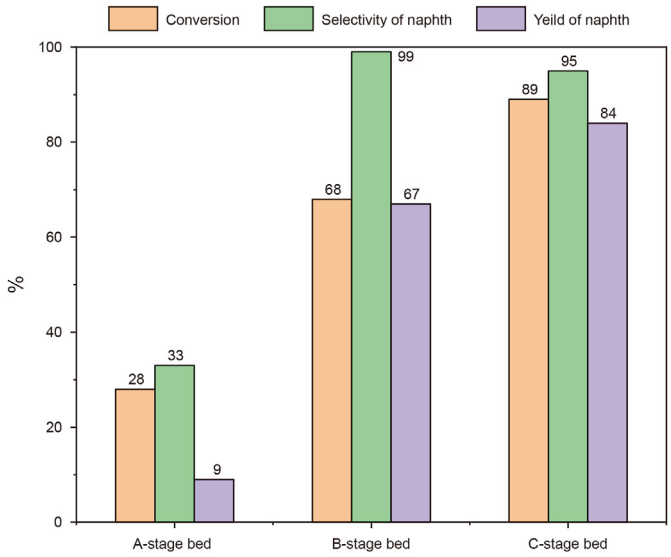

Fig. 8. Diesel hydrocracking activity of A, B, C catalyst bed.

activity reaction evaluation of each bed layer under the same evaluation conditions. The catalyst loading method is shown in Fig. 7.

In the reaction process, the liquid product of bed A is the reaction feedstock of bed B, the liquid product of bed B is the reaction feedstock of bed C. The hydrocracking activities of the catalysts on A, B and C beds are calculated according to the product distribution on each bed, as shown in Fig. 8, the specific composition of feedstock and the liquid products is shown in Fig. 9. Although the acid density and acid strength of the catalyst in bed A, B and C gradually decreased, the diesel conversion and naphtha yield on each bed still increase significantly. It means there is a synergistic effect among the catalysts, which can promote the efficient conversion of diesel to naphtha components.

The content of monocyclic naphthenic hydrocarbons and paraffins hydrocarbons increases after the diesel processed by A-bed catalyst Cat-ASA$_{4.0}$, but the polycyclic aromatic hydrocarbons decreased most significantly, from 5.5% to 1.2%. This means that the catalyst Cat-ASA$_{4.0}$ in A-bed mainly carries out the hydrocracking process of polycyclic aromatic hydrocarbons, the main reactant for hydrogenation process in this reaction. However, the content of polycyclic aromatic hydrocarbons in the feedstock is only 5.5%, so it cannot provide enough feedstock for the high conversion rate of the A-bed catalyst, and it is also the reason for hydrogenation activity of catalyst has little influence on the results of reaction. Moreover, although the bed layer of A is the catalyst Cat-ASA$_{4.0}$ with strong cracking activity, the reaction space velocity is low in the mulit-component catalysts grading system, which shortens the contact time between the reactants and catalyst (Wang et al., 2019). Therefore, the overreaction is controlled (Pastor-Pérez et al., 2018), the ideal reaction process has been suppressed too, and as the result, the conversion of diesel on the A-bed catalyst is only 28%.

A total of about 16.8% of aromatics and polycyclic naphthenic hydrocarbons in the product of A-bed catalyst are hydrocracking on the B-bed catalyst Cat-ASA$_{1.7}$, and the content of monocyclic naphthenic hydrocarbons and paraffins hydrocarbons, the ideal components of naphtha, is significantly increased. The diesel conversion, naphtha selectivity and yield on the B-bed catalyst increase sharply, especially the selectivity of naphtha reaches up 99.0% as

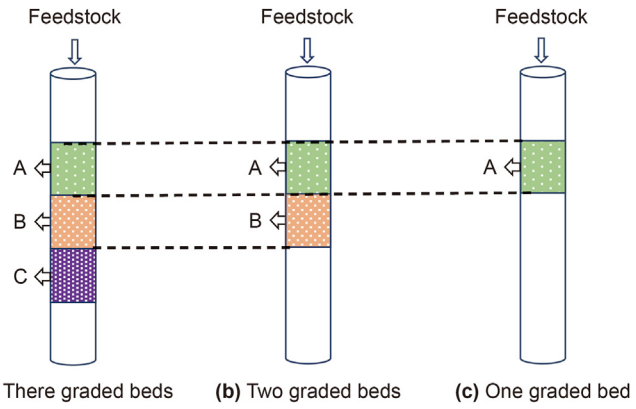

Fig. 7. Loading modes of decreasing bed. (A: Cat-ASA$_{4.0}$; B: Cat-ASA$_{1.7}$; C: Cat-ASA$_{0.7}$).

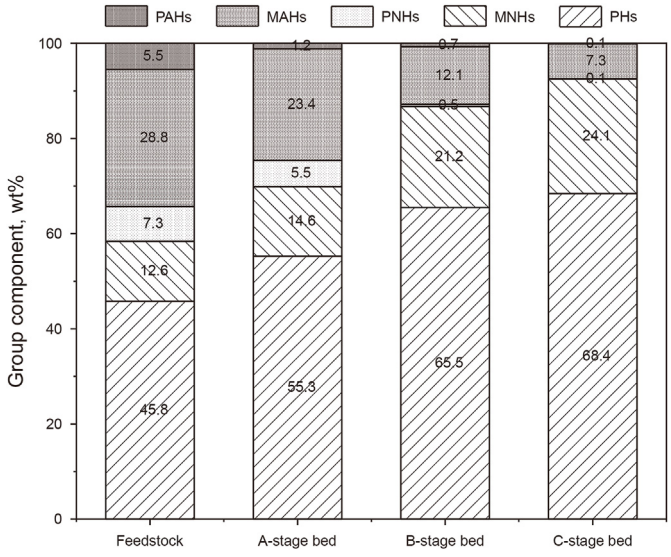

Fig. 9. Composition of liquid products of decreasing bed. (PAHs: Polycyclic Aromatic Hydrocarbons; MAHs: Monocyclic Aromatic Hydrocarbons; PNHs: Polycyclic Naphthenic Hydrocarbons; MNHs: Monocyclic Naphthenic Hydrocarbons; PHs: Paraffins Hydrocarbons).

shown in Fig. 8. It indicates that almost all diesel components in the catalyst B-bed are processed into naphtha, which is consistent with the high naphtha selectivity shown in the single-component catalyst bed.

At this time, the feedstock has been processed by A-bed and B-bed catalyst, the content of ideal component of naphtha, monocyclic naphthenic hydrocarbons and paraffins hydrocarbons, is already very high, but there are still only a small number of aromatics and polycyclic naphthenic hydrocarbons are not completely converted in its composition (Peng et al., 2018). Although the C-bed catalyst Cat-ASA$_{0.7}$ with low acid density and weakly acidity, it uses limited acidic sites to process the residual macromolecules, and on the other hand, it promotes the diffusion of products through large pores to prevent overreaction. Finally, the diesel conversion rate and naphtha selectivity on the C-bed reach to 89% and 95%, respectively. It indicates that most of the products in the B-bed are effectively converted into the naphtha in the C-bed catalyst, which further increases the content of ideal naphtha component in the product.

In summary, due to the competitive adsorption among the molecules of different sizes on the active sites (Guo et al., 2019; Weitkamp, 2012), macromolecules with fused rings are preferentially adsorbed and undergo hydrocracking reactions (Xu et al., 2020; Yue et al., 2017). As the reaction progressing, the composition of feedstock becomes lighter and lighter, and the need for active sites is getting lower and lower, but in order to promote the diffusion of products and prevent them from overreacting, the space needs are increasing.

It can be judged that in the multi-component catalyst grading system, as the reaction space velocity on each layer of catalyst increases, the excessive cracking process is controlled. Furthermore, the active channel with decreasing acidity and the channel structure with increasing size highly match the processing process of diesel hydrocracking to naphtha, and the more the number of graded beds, the higher the matching degree, so the three-component catalyst grading system has the highest catalytic efficiency.

4. Conclusions

In the grading system of multi-component catalyst with acidity decreasing and pore properties increasing in the flow direction of feedstock, the composition of reactants becomes lighter and lighter, but the catalyst can still maintain a high conversion efficiency of feedstock and high selectivity of naphtha. It is due to the loading volume of catalyst decreases, and the reaction space velocity on each catalyst increases, which shortens the contact time between catalyst and feedstock, and effectively controls the excessive reaction. In addition, the pore channels of the catalyst increase, which is conducive to the timely diffusion of the product, preventing its deep cracking, and increasing the content of the naphtha composition in the product.

To sum up, along the direction of feedstock, the catalyst grading system with acidity decreasing and pore structure increasing can satisfy the demand for catalyst activity in the conversion process of changing diesel components to naphtha. Therefore, a catalytic activity channel matching the reaction process has been constructed. Moreover, the number of graded beds is, the higher the matching degree between the catalyst system and the reaction process is, and the more conducive to the efficient conversion of diesel to naphtha components. The three-component catalyst grading system provides guidance for the conversion of feedstock to naphtha, so the selectivity and yield of naphtha are much higher than those of single-component catalysts, and the reaction effect of $1+1+1>3$ is achieved.

Declaration of competing interest

The authors declare that they have no known competing financial interests or personal relationships that could have appeared to influence the work reported in this paper.

Acknowledgments

National Key R&D Program of China (2021YFA1501203) is acknowledged for financial support.

References

Angeles, M., Leyva, C., Ancheyta, J., et al., 2014. A review of experimental procedures for heavy oil hydrocracking with dispersed catalyst. Catal. Today 220, 274–294. https://doi.org/10.1016/j.cattod.2013.08.016.

Azizi, N., Ali, S.A., Alhooshani, K., et al., 2013. Hydrotreating of light cycle oil over NiMo and CoMo catalysts with different supports. Fuel Process. Technol. 109, 172–178. https://doi.org/10.1016/j.fuproc.2012.11.001.

Bellussi, G., Rispoli, G., Landoni, A., et al., 2013. Hydroconversion of heavy residues in slurry reactors: developments and perspectives. J. Catal. 308, 189–200. https://doi.org/10.1016/j.jcat.2013.07.002.

Busca, G., 2019. Catalytic materials based on silica and alumina: structural features and generation of surface acidity. Prog. Mater. Sci. 104, 215–249. https://doi.org/10.1016/j.pmatsci.2019.04.003.

Busca, G., 2020. Silica-alumina catalytic materials: a critical review. Catal. Today. 357, 621–629. https://doi.org/10.1016/j.cattod.2019.05.011.

Cao, Z., Zhang, X., Mei, J., et al., 2022. Hydrocracking straight-run diesel into high-value chemical materials: the effect of acidity and kinetic study. Ind. Eng. Chem. Res. 61 (25), 8685–8697. https://doi.org/10.1021/acs.iecr.2c00262.

Dai, F., Wang, H., Gong, M., et al., 2016. Modeling of kinetic-based catalyst grading for upgrading shale oil hydrogenation. Fuel 166 (6), 19–23. https://doi.org/10.1016/j.fuel.2015.10.089.

De, Jong, Krijn, P., Zečević, J., Friedrich, H., et al., 2010. Zeolite Y crystals with trimodal porosity as ideal hydrocracking catalysts. Angew. Chem. Int. Ed. 49 (52), 10074–10078. https://doi.org/10.1002/anie.201004360.

Derouane, E.G., Védrine, J.C., Pinto, R.R., et al., 2013. The acidity of zeolites: concepts, measurements and relation to catalysis: a review on experimental and theoretical methods for the study of zeolite acidity. Catal. Rev. 55 (4), 454–515. https://doi.org/10.1080/01614940.2013.822266.

Dik, P.P., Klimov, O.V., Koryakina, G.I., et al., 2014. Composition of stacked bed for VGO hydrocracking with maximum diesel yield. Catal. Today. 220–222 (14), 124–132. https://doi.org/10.1016/j.cattod.2013.07.004.

Dik, P.P., Danilova, I.G., Golubev, I.S., et al., 2019. Hydrocracking of vacuum gas oil over NiMo/zeolite-Al_2O_3: influence of zeolite properties. Fuel 237 (19), 178–190. https://doi.org/10.1016/j.fuel.2018.10.012.

Ding, W., Wang, D., Zhao, D., et al., 2016. A novel self-assembled hierarchical-structured catalyst for the diffusion of macromolecules. Aust. J. Chem. 69 (8), 856–864. https://doi.org/10.1071/CH15747.

Feng, W., Zheng, B., Cui, Q., et al., 2022. Influence of ASA composition on its supported Mo catalyst performance for the slurry-phase hydrocracking of vacuum residue. Fuel 324, 124628. https://doi.org/10.1016/j.fuel.2022.124628.

Ge, J., Sun, J., Zhang, P., et al., 2022. Effect of two-component amorphous silica-alumina (ASA) with different Si/Al molar ratios on hydrocracking reactions for increasing naphtha over NiW/USY-ASA. Catal. Sci. Technol. 12, 3695–3705. https://doi.org/10.1039/D2CY00458E.

Guo, S., Vengsarkar, P., Jayachandrababu, K.C., et al., 2019. Aromatics/Alkanes separation: simulated moving bed process model development by a concurrent approach and its validation in a mini-plant. Sep. Purif. Technol. 215, 410–421. https://doi.org/10.1016/j.seppur.2019.01.030.

Guo, W., Kortenbach, T., Qi, W., et al., 2022. Selective tandem catalysis for the synthesis of 5-hydroxymethylfurfural from glucose over *in-situ* phosphated titania catalysts: insights into structure, bi-functionality and performance in flow microreactors. Appl. Catal. B Environ. 301, 120800. https://doi.org/10.1016/j.apcatb.2021.120800.

Hensen, E., Poduval, D., Magusin, P., et al., 2010. Formation of acid sites in amorphous silica-alumina. J. Catal. 269 (1), 201–218. https://doi.org/10.1016/j.jcat.2009.11.008.

Ivanova, I.I., Kuznetsov, A.S., Yuschenko, V.V., et al., 2004. Design of composite micro/mesoporous molecular sieve catalysts. Pure Appl. Chem. 76 (9), 1647–1657. https://doi.org/10.1351/pac200476091647.

Li, H., Duan, X., Wu, X., et al., 2014. Growth of alloy MoS_{2x} $Se_{2\ (1-x)}$ nanosheets with fully tunable chemical compositions and optical properties. J. Am. Chem. Soc. 136 (10), 3756–3759. https://doi.org/10.1021/ja500069b.

Li, T., Zhang, L., Tao, Z., et al., 2020. Synthesis and characterization of amorphous silica-alumina with enhanced acidity and its application in hydro-isomerization/cracking. Fuel 279, 118487. https://doi.org/10.1016/j.fuel.2020.118487.

Licea, Y.E., Amaya, S.L., Echavarría, A., et al., 2014. Simultaneous tetralin HDA and dibenzothiophene HDS reactions on NiMo bulk sulphide catalysts obtained from mixed oxides. Catal. Sci. Technol. 4 (5), 1227–1238. https://doi.org/10.1039/C3CY00801K.

Liu, H., Huang, Z., He, C., et al., 2022. Metal-to-semiconductor transitions in constituent-tunable layered two-dimensional $Nb_xW_{1-x}Se_2$ based on first principles calculations. Phys. E Low-dimens. Syst. Nanostruct. 144, 115388. https://doi.org/10.1016/j.physe.2022.115388.

Liu, J.X., Liu, X.Q., Yan, R.X., et al., 2022. Active phase morphology engineering of $NiMo/Al_2O_3$ through La introduction for boosting hydrodesulfurization of 4, 6-DMDBT. Petrol. Sci. 20 (2), 1231–1237. https://doi.org/10.1016/j.petsci.2022.09.023.

Meng, Q., Liu, B., Piao, J., et al., 2012. Synthesis of the composite material Y/ASA and its catalytic performance for the cracking of *n*-decane. J. Catal. 290, 55–64. https://doi.org/10.1016/j.jcat.2012.03.002.

Miao, P., Zhu, X., Guo, Y., et al., 2021. Combined mild hydrocracking and fluid catalytic cracking process for efficient conversion of light cycle oil into high-quality gasoline. Fuel 292, 120364. https://doi.org/10.1016/j.fuel.2021.120364.

Pastor-Pérez, L., Le Saché, E., Jones, C., et al., 2018. Synthetic natural gas production from CO_2 over Ni-x/CeO_2-ZrO_2 (x = Fe, Co) catalysts: influence of promoters and space velocity. Catal. Today 317, 108–113. https://doi.org/10.1016/j.cattod.2017.11.035.

Peng, C., Guo, R., Fang, X.C., 2016. Improving ultra-deep desulfurization efficiency by catalyst stacking technology. Catal. Lett. 146 (3), 701–709. https://doi.org/10.1007/s10562-015-1675-4.

Peng, C., Cao, Z., Du, Y., et al., 2018. Optimization of a pilot hydrocracking unit to improve the yield and quality of jet fuel together with heavy naphtha and tail oil. Ind. Eng. Chem. Res. 57 (6), 2068–2074. https://doi.org/10.1021/acs.iecr.7b04981.

Peng, C., Liu, B., Feng, X., et al., 2020. Engineering dual bed hydrocracking catalyst towards enhanced high-octane gasoline generation from light cycle oil. Chem. Eng. J. 389, 123461. https://doi.org/10.1016/j.cej.2019.123461.

Peng, C., Liu, P., Zhou, Z., et al., 2022. Detailed understanding on thermodynamic and kinetic features of phenanthrene hydroprocessing on Ni-Mo/HY catalyst. AIChE J. 68 (11), 17831. https://doi.org/10.1002/aic.17831.

Perras, F.A., Wang, Z., Kobayashi, T., et al., 2019. Shedding light on the atomic-scale structure of amorphous silica-alumina and its Brønsted acid sites. Phys. Chem. Chem. Phys. 21 (35), 19529–19537. https://doi.org/10.1039/C9CP04099D.

Popović, Z.M., Souček, I., Ostrovskii, N.M., et al., 2016. Whether integrating refining and petrochemical business can provide opportunities for development of petrochemical industry in Serbia. Hem. Ind. 70 (3), 307–318. https://doi.org/10.2298/HEMIND150122037P.

Pyagay, I.N., Shaidulina, A.A., Konoplin, R.R., et al., 2022. Production of amorphous silicon dioxide derived from aluminum fluoride industrial waste and consideration of the possibility of its use as Al_2O_3-SiO_2 catalyst supports. Catalysts 12 (2), 162. https://doi.org/10.3390/catal12020162.

Saab, R., Polychronopoulou, K., Zheng, L., et al., 2020. Synthesis and performance evaluation of hydrocracking catalysts: a review. J. Ind. Eng. Chem. 89, 83–103. https://doi.org/10.1016/j.jiec.2020.06.022.

Saber, O., Gobara, H.M., 2014. Optimization of silica content in alumina-silica nanocomposites to achieve high catalytic dehydrogenation activity of supported Pt catalyst. Egypt. J. Petrol. 23 (4), 445–454. https://doi.org/10.1016/j.ejpe.2014.11.001.

Sanchez Escribano, V., Garbarino, G., Finocchio, E., et al., 2017. γ-Alumina and amorphous silica-alumina: structural features, acid sites and the role of adsorbed water. Top. Catal. 60 (19–20), 1554–1564. https://doi.org/10.1007/s11244-017-0838-5.

Sihombing, J.L., Gea, S., Wirjosentono, B., et al., 2020. Characteristic and catalytic performance of Co and Co-Mo metal impregnated in sarulla natural zeolite catalyst for hydrocracking of MEFA rubber seed oil into biogasoline fraction. Catalysts 10 (1), 121. https://doi.org/10.3390/catal10010121.

Song, C., 2003. An overview of new approaches to deep desulfurization for ultra-clean gasoline, diesel fuel and jet fuel. Catal. Today 86 (1–4), 211–263. https://doi.org/10.1016/S0920-5861(03)00412-7.

Song, C., Wang, M., Zhao, L., et al., 2013. Synergism between the Lewis and Brønsted acid sites on HZSM-5 zeolites in the conversion of methylcyclohexane. Chin. J. Catal. 34 (11), 2153–2159. https://doi.org/10.1016/S1872-2067(12)60721-9.

Tan, Q., Bao, X., Song, T., et al., 2007. Synthesis, characterization, and catalytic properties of hydrothermally stable macro–meso–micro-porous composite materials synthesized via in situ assembly of preformed zeolite Y nanoclusters on kaolin. J. Catal. 251 (1), 69–79. https://doi.org/10.1016/j.jcat.2007.07.014.

Threlkel, R., Dillon, C., Singh, U.G.U., et al., 2010. Increase flexibility to upgrade residuum using recent advances in RDS/VRDS-RFCC process and catalyst technology. J. Jpn. Petrol. Inst. 2, 65–74. https://doi.org/10.1627/jpi.53.65.

Voiry, D., Yamaguchi, H., Li, J., et al., 2013. Enhanced catalytic activity in strained chemically exfoliated WS_2 nanosheets for hydrogen evolution. Nat. Mater. 12 (9), 850–855. https://doi.org/10.1038/nmat3700.

Wang, C., Jie, X., Qiu, Y., et al., 2019. The importance of inner cavity space within Ni@SiO_2 nanocapsule catalysts for excellent coking resistance in the high-space-velocity dry reforming of methane. Appl. Catal. B Environ. 259, 118019. https://doi.org/10.1016/j.apcatb.2019.118019.

Wang, J., Li, T., Wang, Q., et al., 2020. Controlled growth of atomically thin transition metal dichalcogenides via chemical vapor deposition method. Mater. Today Adv. 8, 100098. https://doi.org/10.1016/j.mtadv.2020.100098.

Wang, X., Arai, M., Wu, Q., et al., 2020. Hydrodeoxygenation of lignin-derived phenolics-a review on the active sites of supported metal catalysts. Green Chem. 22 (23), 8140–8168. https://doi.org/10.1039/D0GC02610G.

Wang, Y., Wang, C., Wang, L., et al., 2021. Zeolite fixed metal nanoparticles: new perspective in catalysis. Acc. Chem. Res. 54 (11), 2579–2590. https://doi.org/10.1021/acs.accounts.1c00074.

Weitkamp, J., 2012. Catalytic hydrocracking-mechanisms and versatility of the process. ChemCatChem 4 (3), 292–306. https://doi.org/10.1002/cctc.201100315.

Weng, X., Cao, L., Zhang, G., et al., 2020. Ultradeep hydrodesulfurization of diesel: mechanisms, catalyst design strategies, and challenges. Ind. Eng. Chem. Res. 59 (49), 21261–21274. https://doi.org/10.1021/acs.iecr.0c04049.

Xu, Y., Zhong, Z., Lu, S., et al., 2020. Monte Carlo simulations of adsorption of thiophene/benzene in NaX and NaY zeolites from model fuel. Ind. Eng. Chem. Res. 59 (35), 15742–15751. https://doi.org/10.1021/acs.iecr.0c02708.

Yan, R., Liu, X., Liu, J., et al., 2023. Modulating the active phase structure of NiMo/Al_2O_3 by La modification for ultra-deep hydrodesulfurization of diesel. AIChE J. 69 (2), e17873. https://doi.org/10.1002/aic.17873.

Yao, N., Xiong, G., Zhang, Y., et al., 2001. Preparation of novel uniform mesoporous alumina catalysts by the sol-gel method. Catal. Today. 68 (1–3), 97–109. https://doi.org/10.1016/S0920-5861(01)00296-6.

Yue, X.M., Wei, X.Y., Zhang, S.Q., et al., 2017. Hydrogenation of polycyclic aromatic hydrocarbons over a solid superacid. Fuel Process. Technol. 161, 283–288. https://doi.org/10.1016/j.fuproc.2017.03.006.

Zhang, S., Liu, D., Deng, W., et al., 2007. A review of slurry-phase hydrocracking heavy oil technology. Energy Fuels 21 (6), 3057–3062. https://doi.org/10.1021/ef700253f.

Zhang, H.Y., Wang, Y.G., Zhang, P.Z., et al., 2013. Preparation of NiW catalysts with alumina and zeolite Y for hydroprocessing of coal tar. J. Fuel Chem. Technol. 41 (9), 1085–1091. https://doi.org/10.1016/S1872-5813(13)60046-8.

Zholobenko, V., Freitas, C., Jendrlin, M., et al., 2020. Probing the acid sites of zeolites with pyridine: quantitative AGIR measurements of the molar absorption coefficients. J. Catal. 385, 52–60. https://doi.org/10.1016/j.jcat.2020.03.003.

Zhou, W., Wei, Q., Zhou, Y., et al., 2018. Hydrodesulfurization of 4, 6-dimethyldibenzothiophene over NiMo sulfide catalysts supported on meso-microporous Y zeolite with different mesopore sizes. Appl. Catal. B Environ. 238, 212–224. https://doi.org/10.1016/j.apcatb.2018.07.042.

Zhu, W., Zheng, G., Cao, S., et al., 2018. Thermal conductivity of amorphous SiO_2 thin film: a molecular dynamics study. Sci. Rep. 8 (1), 1–9. https://doi.org/10.1038/s41598-018-28925-6.